Self-organization, condensation, and annihilation of topological vortices and antivortices in a multiferroic

S. C. Chae[a], Y. Horibe[a], D. Y. Jeong[b], S. Rodan[a], N. Lee[a], and S.-W. Cheong[a,1]

[a]Rutgers Center for Emergent Materials and Department of Physics and Astronomy, Rutgers, The State University of New Jersey, Piscataway, NJ 08854; and [b]Department of Mathematics, Soongsil University, Seoul 156-743, Korea

Edited* by E. Ward Plummer, Louisiana State University, Baton Rouge, LA, and approved October 26, 2010 (received for review August 2, 2010)

The interaction among topological defects can induce novel phenomena such as disclination pairs in liquid crystals and superconducting vortex lattices. Nanoscale topological vortices with swirling ferroelectric, magnetic, and structural antiphase relationships were found in multiferroic h-$YMnO_3$. Herein, we report the discovery of intriguing, but seemingly irregular configurations of a zoo of topological vortices and antivortices. These configurations can be neatly analyzed in terms of graph theory and reflect the nature of self-organized criticality in complexity phenomena. External stimuli such as chemistry-driven or electric poling can induce the condensation and eventual annihilation of topological vortex–antivortex pairs.

The fascinating concept of topological defects permeates ubiquitously our understanding of the early stage universe, hurricanes, quantum matters such as superfluids and superconductors, and also technological materials such as liquid crystals and magnets (1, 2). These topological defects cannot be disentangled in analytically continuous manners. The hot and cold spots of the cosmic microwave background, providing the information of the early stage of the universe, have been considered as cosmological-scale topological defects (1). Vortices in type-II superconductors and superfluids where supercurrent swirls are examples of quantum topological defects (3, 4). Interactions among topological defects and the resulting configurations of numerous topological defects can be associated with various intriguing phenomena such as the hexagonal lattice formation of superconducting vortices (5). In addition, beautiful optical patterns in liquid crystals such as the Schlieren texture of a nematic and the cholesteric fingerprint texture are due to assemblies of topological defects, called disclinations, in ordered arrangements of mesoscopic molecules (6, 7). Large-scale spatial configurations of these topological defects have been investigated only in a limited degree (8–11). Exceptions include the cases of supercurrent vortices or liquid crystals, but they tend to exhibit either trivial or rather irregular configurations.

Graph theory, with its origin in the famous Seven Bridges of Königsberg problem solved by L. Euler in 1736, has become a matured subject, and expanded its scope of applications to many areas with the advance of computers (12). Graphs consist of two sets: a nonempty set of objects (vertices) and a set of the connections (edges) among the objects. Hence, graph theory is a very useful tool to make mathematical models of many real configurational problems in analyzing the nature of underlying connectivity. This theory is widely used in science, engineering, economics, and even in sociology. Examples range from microscopic phenomena such as atomic bonding in chemistry (13) to grander applications such as connectivity of neuron networks of cerebral cortexes (14) and the World Wide Web (15).

New topological defects with simultaneous ferroelectric and magnetic nature have been identified in hexagonal $REMnO_3$ (RE, rare earths) (16)—a multiferroic where ferroelectricity and magnetism coexist and are intriguingly coupled to each other (17–19). Ferroelectricity in $REMnO_3$ is driven by a structural phase transition associated with the mismatch of RE-O and Mn-O layers (20–22). It turns out that a structural trimerization is also induced by the structural transition, and three types (α, β, and γ) of structural antiphase domains can result from the trimerization (23). The topological defect in $REMnO_3$ consists of six neighboring domains in conjunction with a convergence of both structural antiphase and ferroelectric domains accompanying a sense of rotation. One of the important ingredients for the formation of this topological structure is interlocking of structural and antiphase domain walls. Because it has been known that ferroelectric domain walls pin antiferromagnetic domain walls in hexagonal $REMnO_3$ (18), the topological defect is expected to accompany six antiferromagnetic domains with a sense of rotation at low temperatures. Thus, it is legitimate to call it a multiferroic vortex (24). Herein, we report the discovery of the self-organization of topological vortices and antivortices in h-$YMnO_3$ and its rich physical nature. Furthermore, we found that the connectivity, rather than metric properties such as lengths or sizes, of the self-organized complex network exhibits definite regularities and can be neatly analyzed in terms of mathematical graph theory.

Results and Discussion

Using an optical microscope, we have observed an interesting network-like domain pattern on a hexagonal surface of a chemically etched $YMnO_3$ single crystal as shown in Fig. 1*A* (25). At first glance, the domain pattern appears to form in a random and irregular manner. However, upon careful inspection, a landscape of topological order and regularity is revealed, where every closed connected region (face) is surrounded by an "even" number of vertices connected together by edges, exactly three of which are incident on each vertex. The coloring of maps without having adjacent regions in the same color has been considered for a long time, and this process has become an important part of graph theory. The famous four-color theorem states that all regions of every two-dimensional map can be colored with only four colors in a manner that no two adjacent regions have the same color (26). Mathematically, this four-color theorem is restated as "all faces of every planar map can be four-proper-colorable." Note that a planar graph is a graph that can be drawn on the plane without making any crossings of edges except at the vertices. When a map has met certain regularities or rules, the required number of colors can be less than four. This coloring of regions of a pattern has inspired us to understand the rule for the organization of our domain pattern.

We found that every face of Fig. 1*A* can be properly colored using three different colors (light red, light blue, and light green) as shown in Fig. 1*B*. Additionally, focusing only on edges, we found that every edge can also be properly colored with three colors (red, blue, and green) as clearly depicted in the inset of

Author contributions: S.-W.C. designed research; S.C.C., Y.H., S.R., and N.L. performed research; S.C.C., Y.H., D.Y.J., and S.-W.C. analyzed data; and S.C.C., Y.H., and S.-W.C. wrote the paper.

The authors declare no conflict of interest.

*This Direct Submission article had a prearranged editor.

[1]To whom correspondence should be addressed. E-mail: sangc@physics.rutgers.edu.

This article contains supporting information online at www.pnas.org/lookup/suppl/doi:10.1073/pnas.1011380107/-/DCSupplemental.

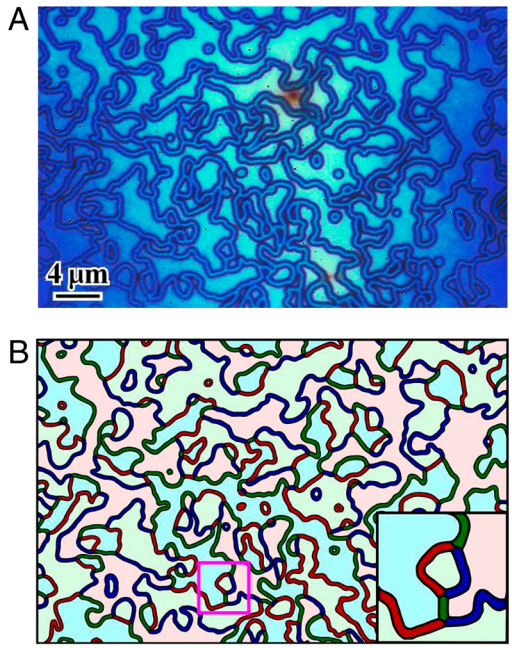

Fig. 1. Ferroelectric domain pattern and coloring of the pattern in $YMnO_3$. (*A*) Ferroelectric domain pattern on the surface of an $YMnO_3$ crystal, imaged using an optical microscope. The upward-polarization and downward-polarization domains of the crystal were etched selectively utilizing phosphoric acid. (*B*) Proper coloring of faces (edges) with three colors; light red (red), light blue (blue), and light green (green). All adjacent edges or faces have different colors. The inset shows an enlarged area, denoted with a pink rectangle, for the clarification of the colors of adjacent edges and faces.

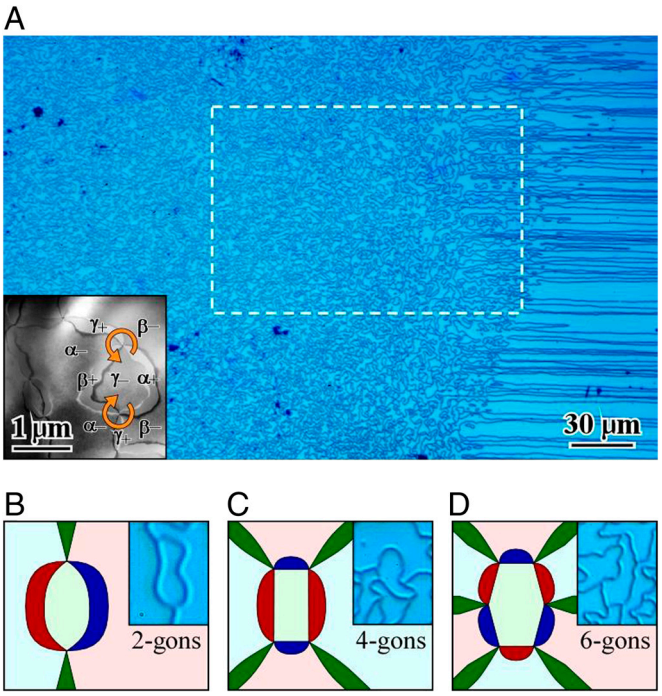

Fig. 2. Various configurations of nanoscale topological vortices and antivortices resulting in a large-scale ferroelectric domain pattern in $YMnO_3$. (*A*) Ferroelectric domain pattern on the surface of a chemical-etched $YMnO_3$ crystal after electric poling imaged, using an optical microscope. The inset shows a dark-field TEM image of an $YMnO_3$ crystal. Six distinguishable domains are merged at one point, and the width of three alternating domains out of six domains is much narrower than that of the other domains. Vorticity of the domain configuration (α^+-β^--γ^+-α^--β^+-γ^- or α^+-γ^--β^+-α^--γ^+-β^-) characterizes vortex vs. antivortex. This TEM image indicates that the dark lines in Fig. 2*A* are narrow domains, rather than walls. (*B–D*) The schematics of two-, four-, and six-gons with one, two, and three vortex–antivortex pairs, respectively. Insets show real examples of two-, four-, and six-gons in Fig. 2*A*.

Fig. 1*B*. A face with N vertices on its boundary is called an N-gon. A K-valent vertex denotes that K edges are incident to the vertex, and a K-valent graph means that all vertices in the graph are K-valent. Then it has been mathematically proven that all faces of a three-valent graph is three-proper-colorable if and only if all faces are composed of even-gons (Table 1) (27). This theorem is certainly consistent with our observation that all faces in Fig. 1*B* are colored with three colors without having adjacent faces in the same color. In addition, all edges of a three-valent graph with even-gons are three-proper-colorable (28), which is also consistent with our observation that all edges in Fig. 1*B* are colored with three colors without having adjacent edges in the same color.

Because $YMnO_3$ is ferroelectric, electric poling, i.e., applying large electric voltages, can change the surface domain patterns. However, we found that the intriguing connectivity of our patterns, i.e., the nature of a three-valent graph with even-gons, remains intact with electric poling. The optical microscope image of the domain pattern after electric poling and chemical etching shown in Fig. 2*A* exhibits a complex network-like pattern of dark lines. The seemingly irregular pattern does form a three-valent planar graph with even-gons, and it exhibits an interesting evolution from the middle (left of Fig. 2*A*) to the edge (right of Fig. 2*A*) of the specimen surface. The complex network-like pattern near the middle becomes less dense and then turns into a curved stripe pattern toward the edge of the specimen. Note that wider-view images of both sides of the specimen are shown in Fig. S1, exhibiting that the curved stripes tend to be perpendicular to the edge of the specimen. It appears that the poling occurs in a highly inhomogeneous manner and no significant poling effect occurs near the middle of the specimen surface. The presence of significant conduction and a large resistivity anisotropy in $YMnO_3$ probably plays an important role in the polarization-flip-related electric discharging (16). The electric discharging, which partially occurs within the specimen, seems to push domains and walls through the crystal edge, which results in the domain pattern with stripes perpendicular to the crystal edge.

Table 1. The number of colors for proper coloring of three- and six-valent planar graphs whose faces (or domains) are all even gons

Valence	Vertex coloring	Edge coloring	Face coloring
3	2	3	3
6	2	6	2

Compared with submicron-scale optical microscope images, transmission electron microscopy (TEM) images with much higher spatial resolution reveal that the network-like domain patterns of $YMnO_3$ form six-valent, rather than three-valent, graphs with even-gons. The TEM dark-field image in the inset of Fig. 2*A*, taken using the $1\bar{3}1$ diffraction spot (the hexagonal $P6_3cm$ notation) of a specimen near the surface of a poled crystal, indicates that the edges or dark lines in the optical microscope image of Fig. 2*A* are indeed narrow domains rather than walls. The TEM image additionally demonstrates that one vertex consists of six distinguishable domains emerging from one point, and that the width of three alternating domains out of six domains is much narrower than the others. Furthermore, each vertex can be identified as a vortex or an antivortex according to its domain vorticity (α^+-β^--γ^+-α^--β^+-γ^- or α^+-γ^--β^+-α^--γ^+-β^-), as shown in the inset of Fig. 2*A* (24). The typical size of these narrow domains in the TEM image is on the order of 100 nm. The atomic force microscope (AFM) image of an etched surface in Fig. S2 shows that the dark lines in Fig. 2*A* are trenches with width of ~130 nm and depth of ~25 nm, which are consistent with the TEM result. Note that because of the different etching rates depending on the polarization direction normal to the surface (29), the upward-

and downward-polarization domains could be different in height after chemical etching. In the case of $YMnO_3$ crystal, the narrow domains have been confirmed to be upward-polarization (+) domains (16). These trenched narrow + domains mean that the + domains were etched faster than downward-polarization (−) domains. Note that the narrow bright lines sandwiched between two dark lines in the optical microscope image in Fig. 1*A* correspond to narrow domains and the dark lines surrounding the bright lines are adjacent walls of the trenches. We have observed the Fig. 1*A*-type images (rather than Fig. 2*A*-type) when a thin layer of liquid remains after chemical etching. Fig. 2 *B*–*D* show the schematic diagram of two-, four-, and six-gons with six-valence, respectively. The insets were taken from the real optical image in Fig. 2*A* for comparison.

Graph theoretical analysis of our patterns alone leads to a number of important conclusions. Mathematically, all vertices of a six-valent planar graph with even-gons are two-proper-colorable (Table 1), and every two-proper-vertex-colorable graph can be considered as a bipartite graph where each vertex can be assigned to one of two disjoint subsets such that each edge connects between one element in one subset and another element in the other subset (30, 31). If one subset is the collection of vortices, then the other subset corresponds to the antivortex collection. Domain patterns we have observed are always six-valent planar graphs with even-gons. This universality, combined with the bipartite nature, demonstrates the following: (*i*) Only two types of vertices (i.e., topological defects) exist, and there are no other types. They are physically topological vortices and antivortices, and any other types of defects do not exist. For example, topological defects such as α^+-β^--"γ^+-α^--γ^+"-β^- or α^+-β^--α^+-β^- do not exist. (*ii*) Any link between vertices is the connection between two different types, which corresponds to the pairing of vortices and antivortices. Any direct links between vortices or antivortices themselves do not exist. An extended view of the dashed area in Fig. 2*A* is shown in Fig. 3*A*, and the schematic of the green-rectangular area in Fig. 3*A* is displayed in Fig. 3*B*. In terms of a six-valent graph, the colored edges in Fig. 3*B* are narrow + domains. The vortex–antivortex pairing is clearly demonstrated in Fig. 3*B* in the sense that all vertices are marked with blue or red dots in a proper manner. Using graph theoretical analysis, we can also conclude that there exists only "three" times "two" types of structural domains. If we consider narrow + domains as edges, a six-valent graph will become a three-valent graph. Then, the fact that all faces (or edges) of a three-valent graph with even-gons are three-proper-colorable (Table 1) means physically that all broad − (or narrow +) domains can be assigned with three types of structural antiphase domains without having adjacent domains in the same structural antiphase. Note that observed domain patterns are always six-valent graphs with even-gons. This universality, combined with above-mentioned graph theoretical analysis, demonstrates that there exists only "three" times "two" types of structural domains. Physically, "three" corresponds to three structural antiphase domains and "two" is related with the presence of ferroelectric + and – domains. We also conclude that there exist no free structural antiphase boundaries or ferroelectric phase boundaries, but they are always interlocked to each other.

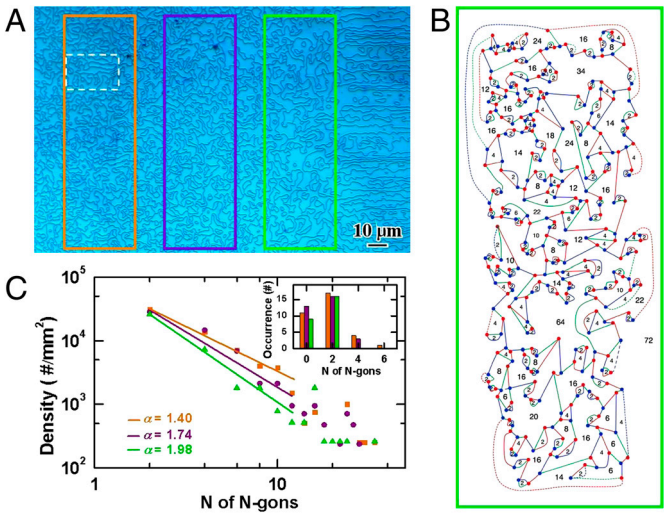

Fig. 3. The electric poling effect of the configuration of numerous topological vortices and antivortices in $YMnO_3$, indicating the annihilation of vortex–antivortex pairs. (*A*) Optical microscopy image of the ferroelectric domain pattern on the surface of a chemical-etched $YMnO_3$ crystal after electric poling—an enlarged area denoted with dashed lines in Fig. 2*A*. The evolution of domain patterns from random to stripe domains is analyzed at the areas shown with orange, blue, and green rectangles. (*B*) Schematic network of dark lines in the green-rectangular area in Fig. 3*A*. The details of this schematic are discussed in *SI Text*, Sect. 3, Fig. S3, and Table S1. (*C*) The power-law distribution of even-gons at the colored-rectangular areas in Fig. 3*A*. Each color for lines and data points matches with that of each rectangle in Fig. 3*A*. The inset shows the distribution of isolated even-gons, including zero-gons without any surrounding vertices (surrounded by one edge).

The statistical distribution of even-gons, shown in Fig. 3*C*, reveals the characteristic of self-organized criticality. The areas enclosed by the orange, purple, and green rectangles in Fig. 3*A* are analyzed in terms of their statistical distribution of even-gons. Note that for the statistical analysis, we have constructed a "finite" planar graph for each rectangular area by adding artificial edges outside of the rectangles in a manner that all vertices are three-valent and all faces are even-gons. It should be emphasized that each area has a number of "isolated" finite graphs, in addition to the main connected graph. These isolated graphs are shown in Fig. S4. As shown in Fig. 3*C*, the distribution of even N-gons in the main graphs shows a power-law behavior ($1/N^a$) with exponent values varying from 1.40 (orange rectangle) to 1.98 (green rectangle). The exponent tends to increase when the domain density decreases, i.e., better poling occurs. The $1/N^a$ ($0 < a < 2$) distribution has been observed in various physical phenomena with self-organized criticality such as the occurrence rate of snow avalanches, earthquakes, and the frequency dependence of noise spectra (32–35). These dissipative systems tend to organize into critical states where the characteristic length and timescales are absent (34). We note that the increase of power-law exponent as the domain density decreases may stem from the increasing effect of the finite size of sampling area, which limits the number of large N-gons. Thus, the intrinsic N-gons distribution for a large sampling area may approach the $1/N$ behavior, resembling the celebrated $1/f$ noise behavior. We would like to emphasize that no one number is special in the N-gon distribution, i.e., there exists no characteristic N-gon. For example, a three-valent graph with "six-gons," exhibiting a honeycomb-like configuration, does have the colorability identical with that of the patterns in Figs. 1*A*, 2*A*, and 3*A*. Thus, paired vortices and antivortices, in principle, can form a three-valent graph with six-gons where one edge corresponds to each pairing. However, there exists nothing special at $N = 6$ in the N-gon distribution. This scale-free behavior truly reflects the unique beauty of our domain patterns and is consistent with the nature of self-organized criticality.

A sequential decomposition of higher-gons into lower-gons upon electric poling can occur through the annihilation of vortex–antivortex pairs (see *SI Text*, Sect. S5 and Fig. S5), and may be responsible for the reduction of the N-gon density as the analyzed area near the stripe domain area. This pair annihilation is accompanied by the disappearance of the narrow domain(s) that connects the vortex and antivortex directly. The sequential decomposition behavior can be also observed in the statistical distribution of the number of even-gons in isolated graphs (see Fig. S4) in various areas, as shown in the inset of Fig. 3*C*. Note

that zero-gons, regions surrounded by only one edge without any vertices, are frequently observed as isolated graphs. These zero-gons are difficult to be removed, possibly due to the lack of the annihilation of vortex–antivortex pairs. It appears that the poling of the zero-gons can be achieved by pushing a part of the edge of zero-gons to the outside of a crystal edge, leading to the formation of a stripe domain pattern near the crystal edge.

It turns out that the presence of "narrow" + domains on the surfaces of $YMnO_3$ crystals, displayed in Figs. 1*A*, 2*A*, and 3*A*, and Fig. S1, is due to a self-poling effect, probably due to oxygen off-stoichiometry near the surfaces (36). In general, hexagonal $REMnO_3$ system exhibits hole-type charge conduction, probably due to cation deficiency or excess oxygen (37). We found that both flat surfaces of as-grown plate-like $YMnO_3$ crystals show narrow domains with upward-polarization near the surfaces (see Fig. S1). On the other hand, when $YMnO_3$ crystals were annealed in oxygen atmosphere at ~900 °C, the + domains and – domains on the surfaces show a roughly 50:50% distribution in the entire area of both flat surfaces. These behaviors can be seen in Fig. 4, where we display three-dimensional illustrations with real AFM images, optical images, and the schematics corresponding to the optical images. In as-prepared crystals, the surfaces, compared with the bulk, tend to have more oxygen vacancies or less oxygen excess, and this reduced oxygen content near surfaces favors energetically the presence of the tail of polarization near surfaces, inducing broad − and narrow + domains near surfaces. This kind of self-poling induced by oxygen off-stoichiometry is well documented in other ferroelectrics (36). Note that the narrow + (broad −) domains on the surfaces of as-grown crystals remain to be narrow (broad) after electric poling even though the overall domain patterns on the surfaces can change as discussed earlier, and the dominant electric poling appears to occur in the interior of crystals (see *SI Text*, Sect. S7 and Fig. S7). Lastly, we emphasize that as the schematic in Fig. 4*C* demonstrates, the roughly 50:50% mixture pattern also shows a six-valent graph with even-gons. However, in this graph, both + and − domains do have various even-gons. On the contrary, the patterns in Figs. 1*A*, 2*A*, and 3*A*, and the schematic in Fig. 4*F* correspond to six-valent graphs where − broad domains show various even-gons, but narrow + domains are always two-gons.

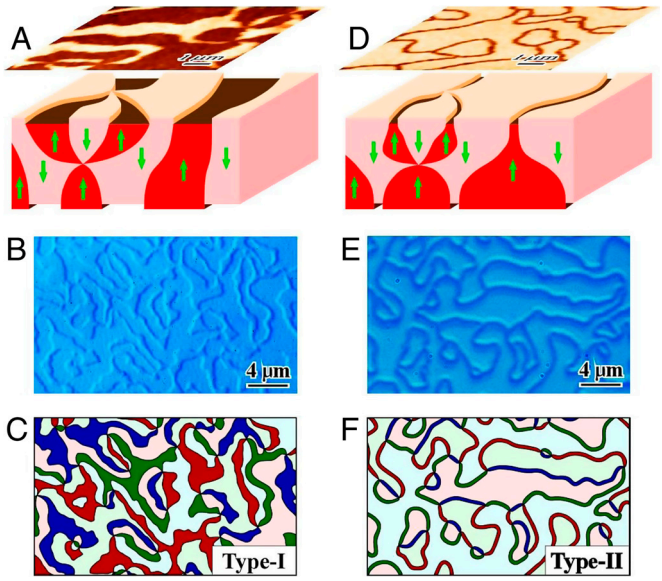

Fig. 4. Two types of the configuration of copious topological vortices and antivortices in $YMnO_3$, demonstrating the condensation of numerous vortex–antivortex pairs. (*A* and *D*) Three-dimensional illustrations of distinct ferroelectric domain structures with real AFM images for O_2-annealed and as-grown $YMnO_3$ crystals, respectively. This difference originates from a chemistry-driven self-poling effect due to the low oxygen content on the surface of as-grown crystals. This self-poling of as-grown crystals favors energetically the presence of wide downward-polarization domains near surfaces. Note that the cartoons also depict vortex or antivortex cores curved along the *c* axis (see *SI Text*, Sect. 6 and Fig. S6). (*B* and *C*) Optical microscope image and a schematic of the surface of an O_2-annelaed $YMnO_3$ crystal after chemical etching, respectively. These pictures show a type-I pattern with a roughly equal distribution of upward- and downward-polarization domains. (*E* and *F*) Optical microscopy image (the area denoted with white dashed lines in Fig. 3*A*) and a schematic of the surface of a self-poled $YMnO_3$ crystal after chemical etching, respectively. These pictures display a type-II pattern with narrow + and broad – domains. The difference between type-I and type-II patterns reflects the condensation of vortex–antivortex pairs.

The domain patterns in $YMnO_3$, where ferroelectricity, magnetism, and structural distortions intertwined to each other, are found to be two types as depicted in Fig. 4: patterns (type I) with the roughly equal distribution of + and − domains, and patterns (type II) with mixtures of narrow + and broad − domains. The formation of type-II patterns stems from chemistry-driven self-poling, and we were able to obtain much larger-range and better-resolution images of type-II patterns than those of type-I patterns, so we have analyzed type-II patterns in great detail, as discussed earlier. Graph theoretical comparison between type-I and type-II patterns indicates the interesting possibility of the condensation of vortex–antivortex pairs, induced by chemistry-driven self-poling. As evident in Fig. 4*C*, type-I patterns form six-valent graphs with even-gons (all possible + even-gons and also all possible − even-gons), the vertices and faces of which are two-proper-colorable. These patterns do have symmetry under the change of + and − signs. On the other hand, type-II patterns correspond to six-valent graphs with all possible − even-gons, but narrow + two-gons only. Self-poling induces the transition from type-I to type-II patterns, and thus the symmetry under the + and − sign change is broken after self-poling. Furthermore, if we consider the narrow two-gons connecting vortices and antivortices as edges, then "the six-valent graph with narrow + two-gons and broad − all-even-gons" can be readily considered as "a three-valent graph with all-even-gons." This compactification of valence can occur only in type-II patterns, not in type-I patterns. High-gons are possibly associated with large energy associated with, e.g., strain, so conceptually they can be considered as excited states, relative to the ground state of two-gons. Unlike type-I patterns, all vortices and antivortices in type-II patterns are paired, i.e., linked by one or two narrow + two-gons, which may result in the lowest total energy.

Therefore, the symmetry breaking under the + and − sign change by self-poling can be considered as "the condensation of topological vortex-antivortex pairs." Note that this condensation, induced by self-poling, can occur through continuous merging of domain walls without changing the number of vortices and antivortices. On the other hand, the electric poling of type-II patterns can induce the vortex–antivortex annihilation as discussed earlier. We found that electric poling of type-I patterns is difficult due to a drastic increase of coercivity and wall pinning after oxygen annealing. Finally, we note that the transition from "+ all even-gons with a power-law distribution of even-gons" to "+ two-gons only" induced by self-poling resembles collapsing a sandpile, in the sense that both may be involved with a process from a self-organized critical state to the ground state induced by external stimulus.

Conclusion

The intriguing ferroelectric and structural antiphase domain patterns in $YMnO_3$ demonstrate the presence of graph-theoretically regular and nontrivial arrangement of numerous topological defects and their response to external stimuli, which can be observed simply under an optical microscope. Graph theoretical consideration of the evolution of the domain patterns to chemistry-driven or electric poling indicates condensation and also annihilation of topological vortices–antivortices pairs induced

by external stimuli. Most of our findings are not possible without the large-range domain images and graph theoretical analysis. Thus, our results undoubtedly provide a paradigm of understanding nontrivial domain patterns in real materials utilizing graph theory.

Materials and Methods

Thin $YMnO_3$ single crystals with a few square millimeters in in-plane size were grown using a flux method with a mixture of 90 mol % of Bi_2O_3 and 10 mol % of $YMnO_3$ powders, which was cooled from 1,200 °C with the rate of 2 °C/h. To observe domain configurations using an optical microscope, thin plate-like crystals with two wide natural facets normal to the crystallographic *c* axis of hexagonal $YMnO_3$ ($P6_3cm$) were etched chemically in phosphoric acid for 30 min at 130 °C. All optical images were taken at room temperature. It turns out that the surfaces with the positively charged head part of electric polarization are etched faster than those with the negatively charged tail part. In order to investigate the role of electric poling on the domain configuration of $YMnO_3$ crystals, we applied a large electric field of ~500 kV/cm, which is significantly larger than the coercive field (~75 kV/cm) of the ferroelectric polarization loop of as-grown $YMnO_3$, to a plate-like specimen with two Ag electrodes (16). After poling, the Ag electrodes were removed mechanically, and then the poled $YMnO_3$ single crystal was etched chemically to reveal domain patterns. The TEM observation was carried out using both JEOL-2010F and JEOL-2000FX TEM on $REMnO_3$ (RE = Y, Ho) single crystals at room temperature. Specimens for dark-field TEM imaging were prepared utilizing Ar ion milling at the liquid-nitrogen temperature. The AFM observation was carried out using a Nanoscope IIIA (Veeco) on the surfaces of chemically etched $YMnO_3$ single crystals.

ACKNOWLEDGMENTS. We would like to thank J. Lebowitz, V. Kiryukhin, and D. Vanderbilt at Rutgers for useful discussions, H. T. Yi and T. Choi at Rutgers for their help for transport measurements, and D. Kwok at Rutgers for critical reading of manuscript. This work was supported by National Science Foundation DMR-0804109. S.C.C. was partially supported by the National Research Foundation of Korea grant funded by the Korean government (NRF-2009-352-C00023).

1. Cruz M, Turok N, Vielva P, Martinez-Gonzalez E, Hobson MA (2007) A cosmic microwave background feature consistent with a cosmic texture. *Science* 318:1612–1614.
2. Mermin ND (1979) The topological theory of defects in ordered media. *Rev Mod Phys* 51:591–648.
3. Abrikosov AA, Gor'kov LP (1961) Contribution to the theory of superconducting alloys with paramagnetic impurities. *Sov Phys JETP* 12:1243–1253.
4. Fisher DS, Fisher MPA, Huse DA (1991) Thermal fluctuations, quenched disorder, phase transitions, and transport in type-II superconductors. *Phys Rev B* 43:130–159.
5. Grigorenko A, Bending S, Tamegai T, Ooi S, Henini MA (2001) A one-dimensional chain state of vortex matter. *Nature* 414:728–731.
6. Lubensky TC, Pettey D, Currier N, Stark H (1998) Topological defects and interactions in nematic emulsions. *Phys Rev E* 57:610–625.
7. Chaikin P, Lubensky T (1995) *Principles of Condensed Matter Physics* (Cambridge Univ Press, Cambridge, UK), pp 495–585.
8. Dandoloff R, Villain-Guillot S, Saxena A, Bishop AR (1995) Violation of self-duality for topological solitons due to soliton-soliton interaction on a cylindrical geometry. *Phys Rev Lett* 74:813–815.
9. Hotta T, Takada Y, Koizumi H, Dagotto E (2000) Topological scenario for stripe formation in manganese oxides. *Phys Rev Lett* 84:2477–2480.
10. Božin ES, Billinge SJL, Kwei GH, Takagi H (1999) Charge-stripe ordering from local octahedral tilts: Underdoped and superconducting $La_{2-x}Sr_xCuO_4$ $(0 \leq x \leq 0.3)$. *Phys Rev B* 59:4445–4454.
11. Bala J, Horsch P, Mack F (2004) Manganites at quarter filling: Role of Jahn-Teller interactions. *Phys Rev B* 69:094415.
12. Wilson RJ (1996) *Introduction to Graph Theory* (Prentice Hall, London), pp 1–99.
13. Balaban AT (1985) Applications of graph theory in chemistry. *J Chem Inf Comput Sci* 25:334–343.
14. Hagmann P, et al. (2008) Mapping the structural core of human cerebral cortex. *PLoS Biol* 6:1479–1493.
15. Barabasi A-L, Albert R (1999) Emergence of scaling in random networks. *Science* 286:509–512.
16. Choi T, et al. (2010) Insulating interlocked ferroelectric and structural antiphase domain walls in multiferroic $YMnO_3$. *Nat Mater* 9:253–258.
17. Ramesh R, Spaldin NA (2007) Multiferroics: Progress and prospects in thin films. *Nat Mater* 6:21–29.
18. Fiebig M, Lottermoser T, Frohlich D, Goltsev AV, Pisarev RV (2002) Observation of coupled magnetic and electric domains. *Nature* 419:818–820.
19. Cheong S-W, Mostovoy M (2007) Multiferroics: A magnetic twist for ferroelectricity. *Nat Mater* 6:13–20.
20. Van Aken BB, Palstra TTM, Filippetti A, Spaldin NA (2004) The origin of ferroelectricity in magnetoelectric $YMnO_3$. *Nat Mater* 3:164–170.
21. Fennie CJ, Rabe KM (2005) Ferroelectric transition in $YMnO_3$ from first principles. *Phys Rev B* 72:100103.
22. dela Cruz C, et al. (2005) Strong spin-lattice coupling in multiferroic $HoMnO_3$: Thermal expansion anomalies and pressure effect. *Phys Rev B* 71:060407.
23. Katsufuji T, et al. (2001) Dielectric and magnetic anomalies and spin frustration in hexagonal $RMnO_3$ ($R = Y$, Yb, and Lu). *Phys Rev B* 64:104419.
24. Mostovoy M (2010) Multiferroics: A whirlwind of opportunities. *Nat Mater* 9:188–190.
25. Safrankova M, Fousek J, Kizaev SA (1967) Domains in ferroelectric $YMnO_3$. *Czech J Phys* 17:559–560.
26. Appel K, Haken W (1976) Every planar map is four colorable. *Am Math Soc Bull* 82:711–712.
27. Wilson R (2001) *Graphs, Colourings and the Four-Colour Theorem* (Oxford Univ Press, New York), pp 38–42.
28. König D (1916) About graph theory and its application to determinants and quantity of teaching. *Math Ann* 77:453–465.
29. Soergel E (2005) Visualization of ferroelectric domains in bulk single crystals. *Appl Phys B: Lasers O* 81:729–751.
30. König D (1990) *Theory of Finite and Infinite Graphs* (Birkhäuser, Boston), pp 345–348.
31. Roberts FS (1984) *Applied Combinatorics* (Prentice Hall, Englewood Cliffs, NJ), pp 97–107.
32. Kirton MJ, Uren MJ (1989) Noise in solid-state microstructures—a new perspective on individual defects, interface states and low-frequency (1/*f*) noise. *Adv Phys* 38:367–468.
33. Weissman MB (1988) 1/*f* noise and other slow, nonexponential kinetics in condensed matter. *Rev Mod Phys* 60:537–571.
34. Bak P, Tang C, Wiesenfeld K (1987) Self-organized criticality: An explanation of the 1/*f* noise. *Phys Rev Lett* 59:381–384.
35. Watts DJ (2002) A simple model of global cascades on random networks. *Proc Natl Acad Sci USA* 99:5766–5771.
36. Wang RV, et al. (2009) Reversible chemical switching of a ferroelectric film. *Phys Rev Lett* 102:047601.
37. Subba Rao G, Wanklyn B, Rao C (1971) Electrical transport in rare earth orthochromites, -manganites and -ferrites. *J Phys Chem Solids* 32:345–358.